Competing effects of Mn and Y doping on the low-energy excitations and phase diagram of $La_{1-y}Y_yFe_{1-x}Mn_xAsO_{0.89}F_{0.11}$ iron-based superconductors

M. Moroni,[1,*] S. Sanna,[1] G. Lamura,[2] T. Shiroka,[3,4] R. De Renzi,[5] R. Kappenberger,[6] M. A. Afrassa,[6,7] S. Wurmehl,[6,8] A. U. B. Wolter,[6] B. Büchner,[6,8] and P. Carretta[1]

[1]*Department of Physics, University of Pavia-CNISM, I-27100 Pavia, Italy*
[2]*CNR-SPIN and Università di Genova, via Dodecaneso 33, I-16146 Genova, Italy*
[3]*Laboratorium für Festkörperphysik, ETH Hönggerberg, CH-8093 Zürich, Switzerland*
[4]*Paul Scherrer Institut, CH-5232 Villigen PSI, Switzerland*
[5]*Department of Physics and Earth Sciences, University of Parma-CNISM, I-43124 Parma, Italy*
[6]*Leibniz-Institut für Festkörper- und Werkstoffforschung (IFW) Dresden, 01171 Dresden, Germany*
[7]*Addis Ababa University, College of Natural Science, Department of Physics, Addis Ababa, Ethiopia*
[8]*Institute for Solid State Physics, Dresden Technical University, TU-Dresden, 01062 Dresden, Germany*

(Received 31 May 2016; revised manuscript received 24 July 2016; published 10 August 2016)

Muon spin rotation (μSR) and ^{19}F nuclear magnetic resonance (NMR) measurements were performed to investigate the effect of Mn for Fe substitutions in $La_{1-y}Y_yFe_{1-x}Mn_xAsO_{0.89}F_{0.11}$ superconductors. While for $y = 0$ a very low critical concentration of Mn ($x = 0.2\%$) is needed to quench superconductivity, as y increases the negative chemical pressure introduced by Y for La substitution stabilizes superconductivity and for $y = 20\%$ it is suppressed at Mn contents an order of magnitude larger. A magnetic phase arises once superconductivity is suppressed both for $y = 0$ and for $y = 20\%$. Low-energy spin fluctuations give rise to a peak in ^{19}F NMR $1/T_1$ with an onset well above the superconducting transition temperature and whose magnitude increases with x. Also the static magnetic correlations probed by ^{19}F NMR linewidth measurements show a marked increase with Mn content. The disruption of superconductivity and the onset of the magnetic ground state are discussed in the light of the proximity of $LaFeAsO_{0.89}F_{0.11}$ to a quantum critical point.

DOI: 10.1103/PhysRevB.94.054508

I. INTRODUCTION

The introduction of impurities in superconductors is a well known approach to probe the local response function and to unravel their intrinsic microscopic properties [1]. Both spinless and paramagnetic impurities perturb the local electronic environment and cause a significant change in the spin polarization around them. When the spin correlations are particularly enhanced, as is the case in the proximity of a quantum critical point (QCP) [2,3], or when the amount of impurities starts to be significant, cooperative effects become relevant and marked changes in the superconducting transition temperature are observed, eventually leading to the appearance of a magnetic order [4]. In the pnictides extensive studies on the effect of impurities on the superconducting ground state have been reported [5–10], and the most dramatic and yet not fully understood effect is induced by Mn for Fe substitution in the optimally electron-doped $LaFeAsO_{0.89}F_{0.11}$ [11]. In this material it is sufficient to introduce a tiny amount of paramagnetic Mn impurities, as low as 0.2%, to fully quench superconductivity. It has been shown that at this doping level there is a divergence of the in-plane correlation length, characteristic of a two-dimensional (2D) antiferromagnetically correlated metal approaching a quantum critical point [11]. This QCP separates the superconducting phase from the magnetic ground state developing at Mn contents above 0.2%. Originally it was suggested that Mn impurities could lead to a shift in the spectral weight of the fluctuations from $(0,\pi)$ (stripe wave vector, we take the square lattice unit cell formed by the nearest neighbor Fe atoms) to (π,π) (Néel wave vector) [12] and accordingly to a suppression of interband pairing processes [13]. However, no evidence of a Néel phase in Mn-doped $LaFeAsO_{0.89}F_{0.11}$ has been ever reported, and recent experiments seem rather to suggest that the magnetic order is still characterized by a stripe collinear arrangement [14]. It is interesting to notice that such a marked effect is observed for $LaFeAsO_{0.89}F_{0.11}$ only, whereas $LnFeAsO_{0.89}F_{0.11}$ with smaller lanthanide ions (e.g., for Ln=Sm) shows a much less dramatic effect and much larger amounts of Mn are needed to suppress superconductivity [15,16].

In this paper we present a study of the effect of Mn doping in $LaFeAsO_{0.89}F_{0.11}$ where La is partially substituted by Y, for doping levels up to 20%. By combining muon spin rotation μSR with superconducting quantum interference device (SQUID) magnetometry we were able to draw the phase diagram of $La_{1-y}Y_yFe_{1-x}Mn_xAsO_{0.89}F_{0.11}$ at fixed Y content as a function of the Mn doping level and at fixed Mn doping as a function of the Y doping level. It is shown that Y doping causes a significant shift of the QCP observed in the $y = 0$ system and that magnetism arises only for $x > 5\%$, for $y = 20\%$. ^{19}F nuclear spin-lattice relaxation measurements evidence the enhancement of low-frequency dynamics already present in the normal phase of the samples without Mn. The mechanism giving rise to the onset of the magnetic phase and the suppression of superconductivity are discussed in the light of recent theoretical models.

II. EXPERIMENTAL METHODS AND RESULTS

Two series of polycrystalline $La_{1-y}Y_yFe_{1-x}Mn_xAsO_{0.89}F_{0.11}$ samples have been studied:

*matteo.moroni01@universitadipavia.it

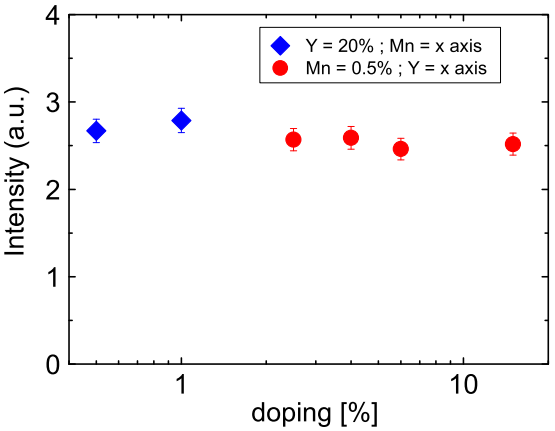

FIG. 1. Intensity of ^{19}F NMR signal at 1.5 T, normalized by the sample mass, at room temperature for selected LaY20 and LaYMn05 samples (see legend).

the first one with fixed $y = 20\%$ yttrium content (LaY20 hereafter) and nominal Mn contents ranging from $x = 0\%$ to 20%, while the second one was prepared with fixed $x = 0.5\%$ Mn content and $y = 0.5\%$, 1%, 5%, 10%, 20%, 23% yttrium contents (LaYMn05 hereafter). The samples were synthesized using a two-step solid-state reaction [17]. Details on sample preparation and characterization by means of powder x-ray diffraction, electron microscopy (SEM), and SQUID magnetometry, used to determine T_c, have been already partially reported in Refs. [18,19]. Electron microscopy WDX revealed that Y and Mn contents are quite close to the nominal ones. All the samples are optimally electron doped with a nominal fluorine content of 11%. The results obtained in the LaY20 series will be compared to those already derived for $LaFe_{1-x}Mn_xAsO_{0.89}F_{0.11}$ (LaY0 hereafter) [11]. It is pointed out that the LaY0 series [5] was not grown with exactly the same procedure as the LaY20 series. Although this may lead to slight changes in the phase diagram this will not affect the analysis and the conclusions presented in this paper.

The intensity of the ^{19}F NMR signal was measured at room temperature in order to check the effective fluorine content both for the LaY20 and for the LaYMn05 series. The results, reported in Fig. 1 show that the absolute fluorine stoichiometry is constant in each sample series within $\pm 0.5\%$.

A. Muon spin relaxation results

In a muon spin relaxation (μSR) experiment 100% spin-polarized positive muons (μ^+) are implanted uniformly into the sample. The $S_\mu = 1/2$ muon spin acts as a magnetic probe, precessing around the local magnetic field B_μ at a frequency $\nu = \gamma_\mu B_\mu / 2\pi$, where $\gamma_\mu = 2\pi \times 135.53$ MHz/T is the muon gyromagnetic ratio. When the muons decay they emit a positron preferentially along the direction of their spins. Hence, by counting the positrons emitted along a given direction one can reconstruct the time dependence of the muon decay asymmetry $A(t)$, proportional to the time evolution of the muon spin polarization [20,21].

In order to probe the local magnetic properties of $La_{1-y}Y_yFe_{1-x}Mn_xAsO_{0.89}F_{0.11}$, zero field (ZF) and

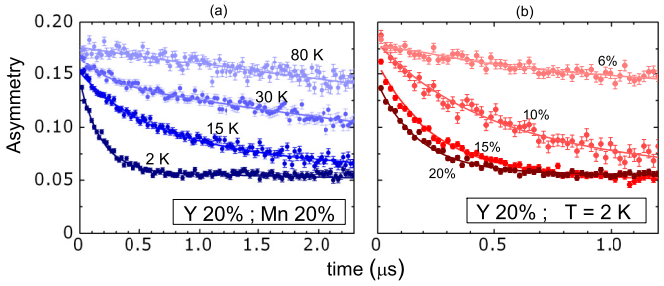

FIG. 2. (a) Zero field μSR signal for the $La_{0.8}Y_{0.2}Fe_{1-x}Mn_xAsO_{0.89}F_{0.11}$ sample with $x = 20\%$, measured at different temperatures. (b) ZF μSR signal for LaY20 samples with $x = 6\%$, 10%, 15%, and 20%, at $T = 2$ K. Solid lines in (a) and (b) represent the best fits to Eq. (1).

longitudinal field (LF) measurements were carried out at the Paul Sherrer Institut (PSI) with the Dolly instrument of SμS facility. ZF measurements are extremely sensitive to spontaneous magnetism since in this configuration the local field at the muon site originates from the internal magnetic order only. On the other hand, LF measurements represent a useful tool to study the spin dynamics and can conveniently be used to distinguish between static and dynamic magnetism [20,21].

Figure 2 shows the typical time dependence of the ZF μSR asymmetry at different temperatures for the samples that display a magnetic order below T_m. The time evolution of the muon asymmetry could be fit with the following standard function:

$$A(t) = A_0[f_\parallel e^{-\lambda_\parallel t} + f_\perp G(t, B_\mu)], \qquad (1)$$

where A_0 is the initial μSR asymmetry, while $f_\parallel$ and $f_\perp$ are the longitudinal ($\mathbf{B}_\mu \parallel \mathbf{S}_\mu$) and transverse ($\mathbf{B}_\mu \perp \mathbf{S}_\mu$) fractions of the asymmetry, respectively. The function $G(t, B_\mu) = \exp(-\lambda_\perp t)$ determines the time dependence of the transverse component, whereas the longitudinal one decays exponentially with a decay rate $\lambda_\parallel$.

At high temperature ($T > 30$ K) the samples of the LaY20 and LaYMn05 series are in the paramagnetic regime and the muon asymmetry can be fit by setting $f_\perp = 0$, with decay rates $\lambda_\parallel \sim 0.09\ \mu s^{-1}$. Upon decreasing the temperature a fast decaying component $f_\perp$ emerges in the LaY20 samples with $x \geqslant 10\%$, evidencing the presence of overdamped oscillations in the muon asymmetry. A similar behavior is observed for samples close to the magnetic superconducting boundary [22,23] and reflects the presence of a significant distribution of local magnetic fields, typically observed when a short range AF magnetic order develops [22]. The size of the internal fields is of the order of the field distribution ΔB_μ, which can be roughly estimated as $\Delta B_\mu = \lambda_\perp / \gamma_\mu$. The values of ΔB_μ obtained from the fit of the data with Eq. (1), of the order of 10 mT, are shown in Fig. 3(a). The static character of the magnetism developing at $T < T_m$ has been confirmed by LF μSR experiment which have shown that a field of about 100 mT is enough to completely recover the initial muon asymmetry at 2 K. At variance, all LaY20 samples with $x < 6\%$ and all the samples of the LYaMn05 series do not display a spontaneous magnetic order down to 2 K.

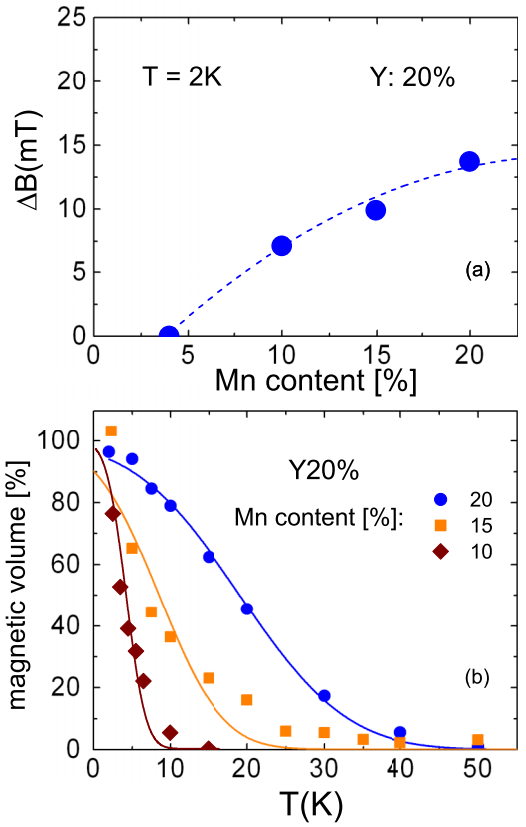

FIG. 3. (a) The values of ΔB at 2 K, for all the samples showing a magnetic order (see Fig. 7), obtained from the fit of the muon asymmetry to Eq. (1). The dashed line is a guide to the eye. (b) The magnetic volume fraction temperature dependence is shown for $y = 20\%$ and $x = 10\%$, 15%, and 20%. The solid lines are best fits to Eq. (2).

The sample magnetic volume fraction V_m, namely the fraction of the sample volume where the muons sense the magnetic order, can be derived from $f_\parallel$. From simple geometric arguments [20,21] it can be shown that in a polycrystalline sample with 100% magnetic volume fraction $f_\parallel = 1/3$ and that in general one can write $V_m(T) = 3/2(1 - f_\parallel(T))$. The temperature dependence of V_m [Fig. 3(b)] shows that the full magnetic volume condition is reached only at low temperatures for all the magnetically ordered samples (LaY20 with $x \geqslant 10\%$). The magnetic ordering temperature can be estimated by fitting $V_m(T)$ to the error function

$$V_m(T) = \frac{1}{2}\left(1 - \mathrm{erf}\left(\frac{T - T_m}{\sqrt{2}\Delta T_m}\right)\right) \quad (2)$$

which assumes the presence of a Gaussian distribution of local transition temperatures centered around the average value T_m. The results are reported in the phase diagram in Fig. 7.

B. Nuclear magnetic resonance results

^{19}F NMR experiments were performed on LaY20 samples in order to complete the study reported in Ref. [18]. The Y for La substitution results in a system with higher chemical pressure with respect to La1111 (La^{3+} and Y^{3+} ionic radii are 103 pm and 90 pm, respectively), without introducing

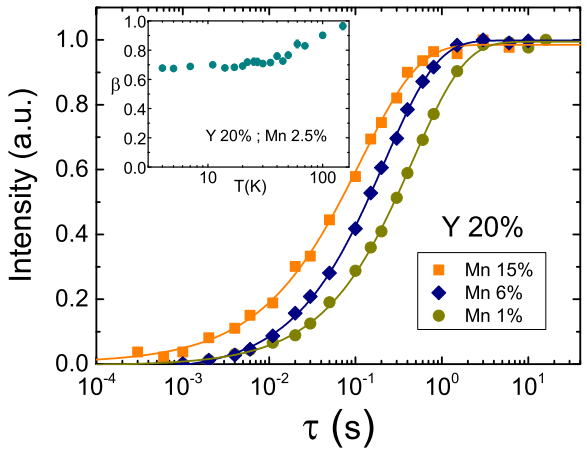

FIG. 4. ^{19}F nuclear magnetization recovery for $La_{0.8}Y_{0.2}Fe_{1-x}Mn_xAsO_{0.89}F_{0.11}$ at 22 K, around the $1/T_1$ peak, for different values of x (see legend). The solid lines are fits to Eq. (3). Inset: temperature dependence of the stretching exponent β used to fit the longitudinal nuclear magnetization recovery for $x = 2.5\%$ and $y = 20\%$.

paramagnetic lanthanide ions, such as Sm^{3+}, which would significantly affect the ^{19}F spin-lattice relaxation rate ($1/T_1$) [24].

The polycrystalline samples were milled to fine powders in order to improve the radiofrequency penetration. All the measurements were performed in a magnetic field of 1.36 T, in the temperature range between 4 K and 100 K. For a few selected samples the temperature range was extended up to 200 K to precisely estimate the high temperature ^{19}F $1/T_1$ trend.

The ^{19}F spin lattice relaxation rate was estimated by fitting the recovery of the longitudinal magnetization $M_z(\tau)$ after a saturation recovery pulse sequence ($\frac{\pi}{2} - \tau - \frac{\pi}{2} - \tau_{\mathrm{echo}} - \pi$). For all the samples the recovery could be nicely fit to a stretched exponential (see Fig. 4):

$$M_z(\tau) = M_0[1 - e^{-(\tau/T_1)^\beta}], \quad (3)$$

with M_0 the nuclear magnetization at thermal equilibrium and β the stretching exponent.

The stretching exponent progressively decreased on cooling below 100 K, and it was found in the range $0.5 \leqslant \beta \leqslant 1$ for all samples (see the inset to Fig. 4). This behavior indicates the presence of a distribution of spin lattice relaxation times which is a common feature of disordered systems, and in our case it is probably due to the different inequivalent impurity configurations resulting from Y and Mn doping. In fact, the low temperature values of β get smaller on increasing the Mn content, namely the number of impurities.

The temperature dependence of $1/T_1$ in LaY20, for Mn contents ranging from $x = 0\%$ up to $x = 20\%$, is shown in Fig. 5. While at high temperature $1/T_1$ displays a linear Korringa behavior (see Ref. [18]) typical of weakly correlated metals, below 80 K the spin lattice relaxation rate progressively increases on cooling, giving rise to a broad peak around 25 K. It is remarked that this increase starts well above T_c or well above T_m, for the magnetically ordered samples. Insights on the nature of the peak can be gained by observing its evolution upon changing the magnitude of the external magnetic field $\vec{H}_0$.

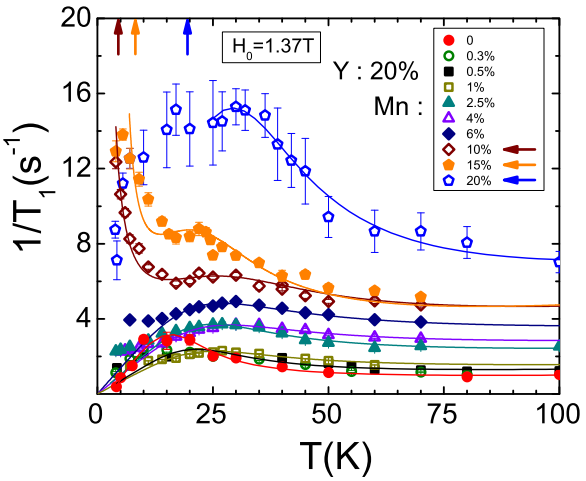

FIG. 5. Temperature dependence of ^{19}F NMR $1/T_1$ for $La_{0.8}Y_{0.2}Fe_{1-x}Mn_xAsO_{0.89}F_{0.11}$ for Mn doping levels up to $x = 20\%$. The solid lines are fits of the data according to Eq. (6) in the text. The arrows indicate T_m for the magnetic samples determined from μSR measurements (from left to right: $x = 10\%$, $x = 15\%$, $x = 20\%$).

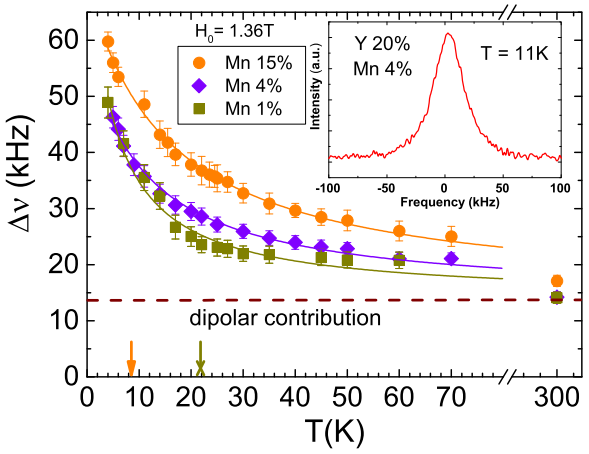

FIG. 6. ^{19}F NMR full width at half intensity for three representative samples of the LaY20 series. Solid lines are best fits according to a Curie-Weiss law while the arrows indicate T_c of the $x = 1\%$ sample (green arrow) and T_m of the $x = 15\%$ sample (orange arrow). Inset: a typical ^{19}F NMR spectrum ($x = 4\%$, $y = 20\%$, $T = 11$ K).

Measurements in a lower field of 0.75 T revealed that while at high temperature $1/T_1$ is only weakly field dependent, the magnitude of the peak at 25 K is significantly enhanced [18], which is exactly the behavior expected for slow dynamics with a characteristic frequency in the MHz range, close to the Larmor frequency ω_0.

The behavior of $1/T_1$ below 25 K depends on the Mn doping level: In samples with Mn doping below 10% the spin lattice relaxation rate decreases with lowering temperature, while for samples with higher Mn doping we observed a steep increase of $1/T_1$ with a divergence at temperatures approaching the magnetic transition temperature determined by μSR. This behavior is associated with the critical divergence of the spin correlation length on approaching the magnetic transition, which yields a power law divergence of $1/T_1 \propto (T - T_m)^{-\alpha}$.

Further insights on the effects of Mn doping can be gained from the study of the temperature dependence of the ^{19}F NMR linewidth $\Delta\nu$, directly related to the amplitude of the staggered magnetization developing around the Mn impurity [10a]. $\Delta\nu$ was derived from the fast Fourier transform of half of the echo signal after a Hahn spin-echo pulse sequence. As can be seen in Fig. 6, by increasing the Mn content a marked increase of $\Delta\nu$ is observed. The data reported were fitted with a Curie-Weiss law $\Delta\nu = (\Delta\nu)_0 + C/(T + \Theta)$ (see solid lines in Fig. 6). The temperature independent term $\Delta\nu_0 \sim 14$ kHz estimated from the fit of the data up to $T = 300$ K is in very good agreement with the value 13.5 kHz estimated for the nuclear dipole-dipole interaction derived from lattice sums. About 80% of the second moment is due to F-La nuclear dipole interaction and about 19.5% to F-F interaction, while only a minor contribution arises from F-As interactions. This term practically does not change by increasing the Mn doping since the lattice parameters change by less than 1.2% between $x = 0$ and $x = 20\%$ [18] and the dipolar contribution of ^{55}Mn nuclei for $x = 20\%$ would cause a change by less than 1% of the linewidth. The results of the fits are summarized in Table I.

TABLE I. Curie constant C and Curie-Weiss temperature θ obtained from the analysis of the temperature evolution of the ^{19}F NMR linewidth $\Delta\nu$ shown in Fig. 6 for $La_{0.8}Y_{0.2}Fe_{1-x}Mn_xAsO_{0.89}F_{0.11}$.

Mn (%)	C (kHz K)	θ (K)
1	300 ± 30	4 ± 1
4	490 ± 20	11 ± 1
15	870 ± 20	16 ± 1

III. DISCUSSION

The phase diagram of LaY20, and for comparison that of LaY0 [11], derived from SQUID magnetization and μSR measurements, are shown in Fig. 7 as a function of Mn

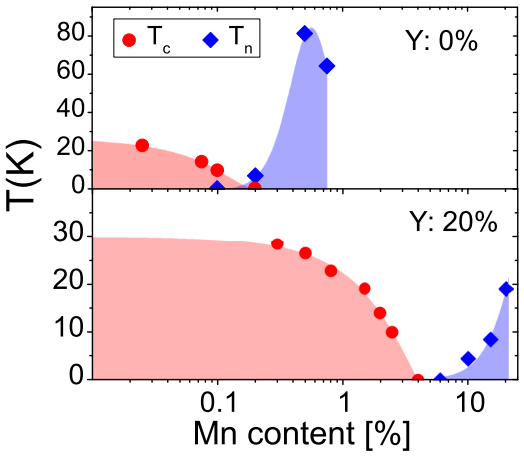

FIG. 7. Phase diagram of $LaFe_{1-x}Mn_xAsO_{0.89}F_{0.11}$ (top) and of $La_{0.8}Y_{0.2}Fe_{1-x}Mn_xAsO_{0.89}F_{0.11}$ (bottom). The red and blue shaded areas are the superconductive and the magnetic phases, respectively. The magnetic transition temperature (blue diamonds) was determined by ZF-μSR while the superconducting transition temperature T_c (red circles) was determined from SQUID magnetization measurements.

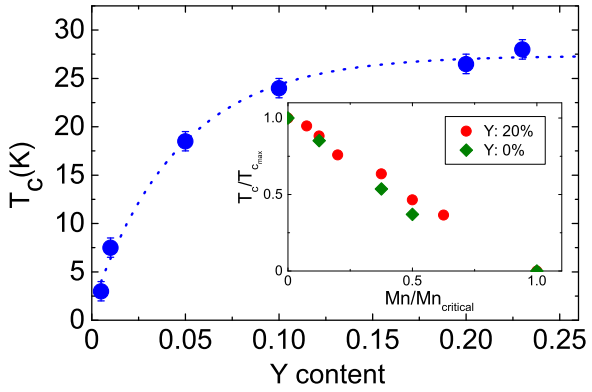

FIG. 8. Critical temperatures for the LaYMn05 samples studied in this paper. The dashed line is a guide to the eye. Inset: $T_c(x)/T_c(x = 0)$ versus the Mn content normalized by the critical content causing the vanishing of T_c for LaY20 and LaY0 (Ref. [11]) series (see text).

content. These data show that the substitution of La with Y causes a sizable increase of the critical Mn threshold x_c required to suppress superconductivity, with an increase from 0.2% to 4% on increasing the Y content from 0 to 20%. In the latter system the threshold is comparable to the one observed [15,16] when smaller paramagnetic ions fully substitute La, namely one has $x_c = 4$ and 8% for $Ln =$ Nd and Sm, respectively. The results on LaY20, where La is partially substituted by the smaller but nonmagnetic Y ion, clearly evidence that the electronic properties of the $LaFeAsO_{0.89}F_{0.11}$ are significantly affected by the chemical pressure or strain induced by the different radii of the lanthanide ions on the FeAs planes. The effect of the chemical pressure is further evidenced in Fig. 8 showing T_c as a function of the La/Y substitution in $La_{1-y}Y_yFe_{0.995}Mn_{0.005}AsO_{0.89}F_{0.11}$. Superconductivity, suppressed by the tiny quantity of 0.5% of Mn for the end $y = 0$ member, is gradually restored by increasing the Y content or, in other terms, the chemical pressure.

When superconductivity is fully suppressed a magnetic order arises both in the LaY0 and in the LaY20 series, as shown in Fig. 7. This behavior suggests that the two orders are competing and that for LaY0 a quantum critical point is separating the superconducting and magnetic phases, as supported by the previous [11] analysis of the temperature dependence of the magnetic correlation length. On the other hand, it should be pointed out that for LaY20 a crossover region where both T_c and T_m are zero is observed for $4\% < x < 6\%$.

The onset of a magnetic order for just 0.2% of Mn in LaY0 indicates that in this compound significant electronic correlations must be present. If the ratio between Hubbard repulsion and the hopping integral associated with the ith band U/t_i is sizable, a significant enhancement of the local spin susceptibility occurs [25]. In the iron-based superconductors quite different behaviors may be observed for the electrons in the five bands crossing the Fermi level and Hund's coupling may even lead to orbital selective Mott transitions [26]. However, for simplicity in the following discussion we will consider that in $LaFeAsO_{0.89}F_{0.11}$ the behavior can be described by an average value of U/t. If U/t is close to a critical value leading to charge localization, the amplitude and the extension of the spin polarization around the Mn impurity significantly increase with respect to a weakly correlated metal [25] and even a tiny amount of impurities may drive the system towards a magnetic ground state. Hence, the undoped $LaFeAsO_{0.89}F_{0.11}$ superconductor must be very close to a QCP since a significant change in the electronic properties occurs by perturbing the system with tiny Mn amounts. This aspect is further supported by the charge localization observed in the LaY0 for Mn contents above x_c and by the significant changes in the c axis lattice parameter [5]. Moreover, as we have previously mentioned, we found that the behavior of the spin correlation length is that expected for a two-dimensional antiferromagnet close to a QCP [11]. Hence the quenching of superconductivity should not be ascribed to a pair breaking effect, where the suppression of superconductivity yields the recovery of the normal metallic state, but to a quantum phase transition affecting the LaY0 electronic ground state.

The chemical pressure induced by Y doping causes an increase in the metallic character since the hopping integral t is enhanced by shrinking the cell. It is clear that when the system becomes more metallic an increased screening of the Coulomb potential is expected and hence also U should be effectively reduced resulting in a decrease in U/t with increasing Y content. Accordingly, the spin polarization around the Mn impurity is reduced and larger Mn contents are needed to induce a magnetic order which, in any case, appears to be characterized by an order parameter which is weaker than that observed in the LaY0 system (Fig. 7). However, the behavior of the LaY0 and LaY20 series becomes similar (see the inset of Fig. 8) once the phase diagram is rescaled by the critical Mn content x_c and the superconducting transition temperature for $T_c(x = 0)$. Namely the Mn doping level x_c yielding the quantum critical point is renormalized by the decrease in U/t.

Further insights on the effect of Mn in LaY0 and LaY20 can be derived from the analysis of the ^{19}F NMR spin-lattice relaxation rate. As it is shown in Fig. 5 a broad peak in $1/T_1$, which is increasing with the Mn content, is detected around 25 K. That peak, observed both in the LaY0 and in the LaY20 series, is a very general feature of these systems since it is present both in superconducting and magnetic samples and also in the sample without Mn doping [18,27], although slightly shifted to lower temperatures. The introduction of increasing Mn contents gives rise to a progressive enhancement of the peak magnitude, suggesting that the presence of paramagnetic impurities strengthens the low-frequency dynamics already present in the pure compound. Its dependence on the magnetic field intensity [18] indicates that it has to be associated with low-frequency fluctuations (MHz range). This peak should not be ascribed to the slowing down of the critical fluctuations on approaching T_m, which are present only in the magnetic samples and give rise to a steeper increase in $1/T_1$ only at lower temperatures (Fig. 5).

The approach devised by Bloembergen-Purcell-Pound [28] (BPP model) is often suited to describe $1/T_1$ in the presence of hyperfine field $\vec{h}(t)$ fluctuations approaching the Larmor frequency ω_0, namely in the MHz range. The model assumes that the autocorrelation function for the field fluctuations decays exponentially:

$$\langle h_\perp(t+\tau)h_\perp(t)\rangle = \langle h_\perp^2\rangle e^{-t/\tau_c}, \quad (4)$$

where τ_c is the characteristic time of the fluctuations and $h_\perp$ is the component of the local fluctuating hyperfine field perpendicular to $\vec{H}_0$, with $\langle h_\perp^2 \rangle$ its mean square amplitude. The spin lattice relaxation rate, which probes the spectral density at ω_0, then takes the form:

$$\frac{1}{T_1} = \gamma^2 \langle h_\perp^2 \rangle \frac{\tau_c(T)}{1 + \omega_0^2 \tau_c(T)^2}, \tag{5}$$

where γ is the nuclear gyromagnetic ratio. In many disordered systems, including cuprates [29], $\tau_c(T)$ is described by a thermally activated law $\tau_c(T) = \tau_0 \exp(E_a/T)$, where E_a is the energy barrier and τ_0 the correlation time at infinite temperature. However, monodispersive fluctuations cannot explain the broad peaks observed in Mn doped compounds. A much better result can be obtained by considering a distribution of energy barriers, and thus of correlation times, associated with the irregular distribution of Mn impurities.

For simplicity, the energy barrier distribution was taken as squared, centered around E_a and with a width Δ. Accordingly Eq. (5) takes the form [30]:

$$\frac{1}{T_1} = \frac{\gamma^2 \langle h_\perp^2 \rangle T}{2\omega_0 \Delta} [\arctan(\omega_0 \tau_0 e^{(\langle E_a \rangle + \Delta)/T}) - \arctan(\omega_0 \tau_0 e^{(\langle E_a \rangle - \Delta)/T})] + cT, \tag{6}$$

where a linear Korringa-like term cT was added to account for the high temperature behavior. Equation (6) was used to fit the $1/T_1$ data for all samples with Mn contents lower than 8%, while for samples with higher Mn doping a term proportional to $(T - T_m)^{-\alpha}$ was added to account for the divergence of $1/T_1$ at the magnetic phase transition. As is shown in Fig. 5 the $1/T_1$ data can be suitably fit to Eq. (6), with the parameters reported in Fig. 9. For the $x = 20\%$ sample the divergence due to magnetic ordering and broad BPP peak overlap making it impossible to obtain a reliable fit on the whole temperature range so only the high temperature data were fitted to Eq. (6). The critical exponent was found to be $\alpha \simeq 1$ both for $x = 10\%$ and for $x = 15\%$. Since in quasi-2D antiferromagnets $1/T_1 \sim \xi^z$ [31], with $\xi \propto (T - T_m)^{-\nu}$ the spin correlation length and z and ν scaling exponents close to the unity [32], the value derived for α appears to be quite reasonable.

The fit parameters shown in Fig. 9 evidence that the mean value of the energy barrier E_a is nearly constant as a function of Mn and that the variation of the correlation time τ_0 of the spin fluctuations is small, in the range of 0.1–0.4 ns. In the LaY0 series Δ increases with x suggesting that the Mn leads to a distribution of activation energies which reflects a strong inhomogeneous electronic environment, even at very small Mn doping levels. For the LaY20 system this distribution is nearly constant and affected by the disorder induced by the large amount of Y introduced in the system. The most significant change is the increase in the amplitude of the local fluctuating field $(\langle h_\perp^2 \rangle)^{1/2}$ with x, which indicates that the strength of the local spin susceptibility in the FeAs plane becomes progressively enhanced by Mn doping. The enhancement of the local spin susceptibility is further supported by the analysis of the temperature dependence of the ^{19}F NMR linewidth (Fig. 6), which is directly related to the amplitude of the staggered magnetization developing around the impurity.

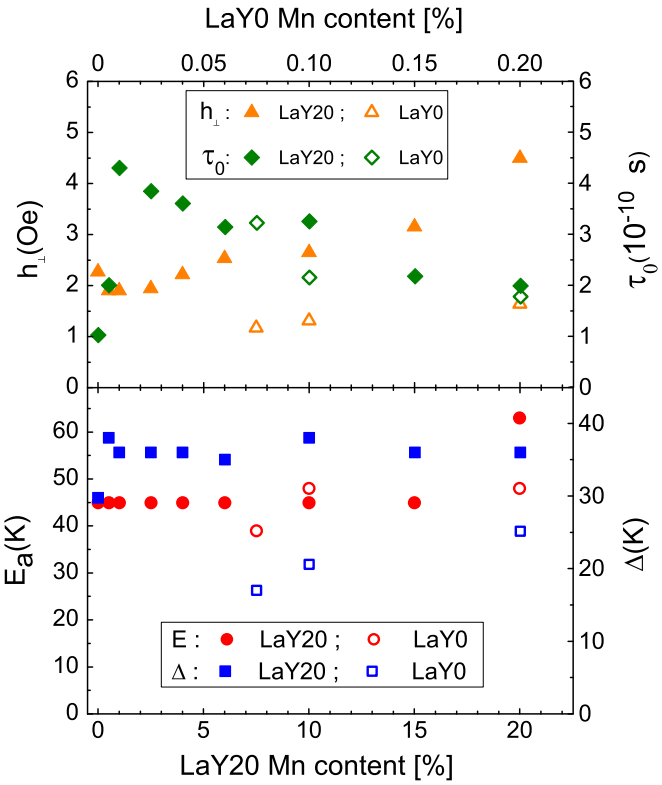

FIG. 9. Parameters extracted from the fit of $1/T_1$ to Eq. (6) as a function of the Mn content for the LaY20 series (filled symbols, bottom horizontal axes) and for the LaY0 series (open symbols, top horizontal axes). Top panel: mean value of the local fluctuating magnetic field $h_\perp$ (left) and correlation time τ_0 (right). Bottom panel: energy barrier E_a (left) and width of the energy barrier distribution Δ (right).

The results, summarized in Table. I, show that both the Curie constant and the Curie-Weiss temperature increase as a function of Mn, indicating that the insertion of Mn strengthens the spin correlations.

The origin of the low-energy fluctuations giving rise to the peak in ^{19}F NMR $1/T_1$ is not yet clear. They seem to be intrinsic to the system since they are detected also for the LaY20 compound without manganese. Furthermore the related activation energies E_a and correlation time τ_0 are almost insensitive to the Mn content indicating that the low-frequency dynamics is nearly unaltered when approaching the disruption of superconductivity. Bumps in the $1/T_1$ vs T behavior have also been detected in other optimally electron-doped iron-based superconductors [27,33–35] in the same T range where the peak in ^{19}F NMR $1/T_1$ arises in Fig. 5. They have been tentatively associated with nematic fluctuations [34] or with the motion of domain walls separating nematic phases [35]. In this scenario the energy barrier E_a may be related to the one separating the degenerate nematic phases [36], and the enhancement of the low-frequency dynamics could be associated with the pinning of those fluctuations by impurities. These dynamics do not seem to be involved in the superconducting mechanism since they survive well above the critical threshold x_c for the suppression of T_c.

IV. CONCLUSIONS

We have shown that Y for La substitution in the optimally electron doped $LaFe_{1-x}Mn_xAsO_{0.89}F_{0.11}$ superconductor leads to a shift in the QCP driven by Mn to doping levels much higher than the ones detected in the series without Y. This shift is associated with an increase in the chemical pressure which causes a decrease in the electronic correlations by Y doping, namely in the ratio U/t. Both in the LaY0 and LaY20 series Mn is observed to enhance low-frequency fluctuations in the MHz range which are already present in the normal phase of the Mn and Y free superconductor. These low energy fluctuations are signaled by a peak in $1/T_1$ which is observed in different families of iron-based superconductors and whose origin still has to be clarified.

ACKNOWLEDGMENTS

Brian Andersen and Maria Gastiasoro are thanked for useful discussions. This work was supported by MIUR-PRIN2012 Project No. 2012X3YFZ2. This work has been supported by the Deutsche Forschungsgemeinschaft through the Priority Programme SPP1458 (Grant No. BE1749/13), SFB 1143, under Grant No. DFG-GRK1621, and through the Emmy Noether Programme WU595/3-1 (S.W.).

[1] H. Alloul, J. Bobroff, M. Gabay, and P. J. Hirschfeld, Rev. Mod. Phys. **81**, 45 (2009).
[2] J. A. Hertz, Phys. Rev. B **14**, 1165 (1976).
[3] S. Sachdev, *Quantum Phase Transitions* (Cambridge University Press, Cambridge, 1999).
[4] J. S. Parker, D. E. Read, A. Kumar, and P. Xiong, Europhys. Lett. **75**, 950 (2006).
[5] M. Sato and Y. Kobayashi, Solid State Commun. **152**, 688 (2012).
[6] E. Satomi, S. C. Lee, Y. Kobayashi, and M. Sato, J. Phys. Soc. Jpn. **79**, 094702 (2010).
[7] S. C. Lee, E. Satomi, Y. Kobayashi, and M. Sato, J. Phys. Soc. Jpn. **79**, 023702 (2010).
[8] S. Sanna, P. Carretta, P. Bonfá, G. Prando, G. Allodi, R. De Renzi, T. Shiroka, G. Lamura, A. Martinelli, and M. Putti, Phys. Rev. Lett. **107**, 227003 (2011).
[9] S. Sanna, P. Carretta, R. De Renzi, G. Prando, P. Bonfà, M. Mazzani, G. Lamura, T. Shiroka, Y. Kobayashi, and M. Sato, Phys. Rev. B **87**, 134518 (2013).
[10] (a) D. LeBoeuf, Y. Texier, M. Boselli, A. Forget, D. Colson, and J. Bobroff, Phys. Rev. B **89**, 035114 (2014); (b) Y. Texier, Y. Laplace, P. Mendels, J. T. Park, G. Friemel, D. L. Sun, D. S. Inosov, C. T. Lin, and J. Bobroff, Europhys. Lett. **99**, 17002 (2012).
[11] F. Hammerath, P. Bonfá, S. Sanna, G. Prando, R. De Renzi, Y. Kobayashi, M. Sato, and P. Carretta, Phys. Rev. B **89**, 134503 (2014).
[12] G. S. Tucker, D. K. Pratt, M. G. Kim, S. Ran, A. Thaler, G. E. Granroth, K. Marty, W. Tian, J. L. Zarestky, M. D. Lumsden, S. L. Bud'ko, P. C. Canfield, A. Kreyssig, A. I. Goldman, and R. J. McQueeney, Phys. Rev. B **86**, 020503 (2012).
[13] R. M. Fernandes and A. J. Millis, Phys. Rev. Lett. **110**, 117004 (2013).
[14] M. Moroni (unpublished).
[15] M. Sato, Y. Kobayashi, S. C. Lee, H. Takahashi, E. Satomi, and Y. Miura, J. Phys. Soc. Jpn. **79**, 014710 (2010).
[16] S. J. Singh, J. Shimoyama, A. Yamamoto, H. Ogino, and K. Kishio, Physica C **494**, 57 (2013).
[17] A. Alfonsov, F. Murányi, V. Kataev, G. Lang, N. Leps, L. Wang, R. Klingeler, A. Kondrat, C. Hess, S. Wurmehl, A. Köhler, G. Behr, S. Hampel, M. Deutschmann, S. Katrych, N. D. Zhigadlo, Z. Bukowski, J. Karpinski, and B. Büchner, Phys. Rev. B **83**, 094526 (2011).
[18] F. Hammerath, M. Moroni, L. Bossoni, S. Sanna, R. Kappenberger, S. Wurmehl, A. U. B. Wolter, M. A. Afrassa, Y. Kobayashi, M. Sato, B. Büchner, and P. Carretta, Phys. Rev. B **92**, 020505(R) (2015).
[19] R. Kappenberger, F. Hammerath, P. Rousse, M. A. Afrassa, H. M. Haghighi, S. Kamusella, G. Prando, G. Lamura, A. U. B. Wolter, M. Moroni, S. Sanna, P. Carretta, C. Hess, H. J. Grafe, H. H. Klauß, S. Wurmehl, and B. Büchner (unpublished).
[20] A. J. Drew, F. L. Pratt, T. Lancaster, S. J. Blundell, P. J. Baker, R. H. Liu, G. Wu, X. H. Chen, I. Watanabe, V. K. Malik, A. Dubroka, K. W. Kim, M. Rossle, and C. Bernhard, Phys. Rev. Lett. **101**, 097010 (2008).
[21] A. Yaouanc and P. D. de Réotier, *Muon Spin Rotation, Relaxation, and Resonance: Applications to Condensed Matter* (Oxford University Press, Oxford, 2011).
[22] P. Carretta, R. De Renzi, G. Prando, and S. Sanna, Phys. Scr. **88**, 068504 (2013).
[23] G. Prando, O. Vakaliuk, S. Sanna, G. Lamura, T. Shiroka, P. Bonfa, P. Carretta, R. De Renzi, H.-H. Klauss, C. G. F. Blum, S. Wurmehl, C. Hess, and B. Büchner, Phys. Rev. B **87**, 174519 (2013).
[24] G. Prando, P. Carretta, A. Rigamonti, S. Sanna, A. Palenzona, M. Putti, and M. Tropeano, Phys. Rev. B **81**, 100508 (2010).
[25] M. N. Gastiasoro and B. M. Andersen, Phys. Rev. Lett. **113**, 067002 (2014); M. N. Gastiasoro, F. Bernardini, and B. M. Andersen, arXiv:1606.09495.
[26] L. dé Medici, G. Giovannetti, and M. Capone, Phys. Rev. Lett. **112**, 177001 (2014).
[27] F. Hammerath, U. Grafe, T. Kühne, H. Kühne, P. L. Kuhns, A. P. Reyes, G. Lang, S. Wurmehl, B. Buchner, P. Carretta, and H.-J. Grafe, Phys. Rev. B **88**, 104503 (2013).
[28] N. Bloembergen, E. M. Purcell, and R. V. Pound, Phys. Rev. **73**, 679 (1948).
[29] M.-H. Julien, A. Campana, A. Rigamonti, P. Carretta, F. Borsa, P. Kuhns, A. P. Reyes, W. G. Moulton, M. Horvatic, C. Berthier, A. Vietkin, and A. Revcolevschi, Phys. Rev. B **63**, 144508 (2001).
[30] M. Filibian, P. Carretta, T. Miyake, Y. Taguchi, and Y. Iwasa, Phys. Rev. B **75**, 085107 (2007).
[31] P. Carretta, A. Rigamonti, and R. Sala, Phys. Rev. B **55**, 3734 (1997).

[32] H. Benner and J. P. Boucher, in *Magnetic Properties of Layered Transition Metal Compounds*, edited by L. J. De Jongh (Kluwer Academic Publisher, Dordrecht, 1990).
[33] L. Bossoni, P. Carretta, W. P. Halperin, S. Oh, A. Reyes, P. Kuhns, and P. C. Canfield, Phys. Rev. B **88**, 100503 (2013).
[34] A. P. Dioguardi, M. M. Lawson, B. T. Bush, J. Crocker, K. R. Shirer, D. M. Nisson, T. Kissikov, S. Ran, S. L. Budko, P. C. Canfield, S. Yuan, P. L. Kuhns, A. P. Reyes, H.-J. Grafe, and N. J. Curro, Phys. Rev. B **92**, 165116 (2015).
[35] L. Bossoni, M. Moroni, M. H. Julien, H. Mayaffre, P. C. Canfield, A. Reyes, W. P. Halperin, and P. Carretta, Phys. Rev. B **93**, 224517 (2016).
[36] R. M. Fernandes and J. Schmalian, Supercond. Sci. Technol. **25**, 084005 (2012).